Experimental and CFD Study of Various Flow Control Techniques on NACA-0012 Airfoil

Aibek Tashtanaliev[1], Gaojun Yu[2], Ramit Rakesh[3], and Sajeed Hussain Shaik[4]
ISAE-Supaero, Toulouse, France, 31400

The present study deals with various flow control techniques on a NACA-0012 airfoil in a transitional Reynolds's number of 8.0e4, at which the flow over the airfoil is mostly laminar and prone to separation over higher angle of attacks. The effectiveness of the flow devices like boundary layer tapes/tube, gurney flap, leading edge serrations, and vortex generators are studied both experimentally and numerically with an aim to trigger the boundary layer to transition, delay the separation and increase the lift. It is found that the gurney flap is effective in increasing the lift, the vortex generators are effective at lower AoA. The leading edge serrations are helpful in delaying the separation and slight increase in lift at cost of increased drag at lower AoA.

Nomenclature

AoA = Angle of Attack (degrees)
d = cylinder diameter
C_p = pressure coefficient
C_l = lift coefficient
C_d = drag coefficient
C = force coefficient in the x direction
Cy = force coefficient in the y direction
c = chord
dt = time step
TE = airfoil's trailing-edge
LE = airfoil's leading-edge
GF = Gurney Flap

[1] Master Student, DAEP, Aibek.TASHTANALIEV@student.isae-supaero.fr.
[2] Master Student, DAEP, Gaojun.YU@student.isae-supaero.fr
[3] Master Student, DAEP, Ramit.RAKESH@student.isae-supaero.fr
[4] Master Student, DAEP, Sajeed-hussain.SHAIK@student.isae-supaero.fr.

I. Introduction

NACA 0012 airfoil has been extensively used in various applications, ranging from aircraft wings and propellers to wind turbine blades and hydrofoils. Its symmetrical shape and predictable aerodynamic characteristics make it suitable for a wide range of purposes, including low and high speed applications. Hence, this airfoil can act as a perfect baseline to test various flow control techniques that aim to reduce flow phenomena such as boundary layer separation or separation bubble that may negatively affect the aerodynamic performance.

II. Experimental Setup

A. Experimental Equipment

Throughout this course we had been working on two wind tunnels namely: 'Pressure setup' - Pitot tubes; and 'Force setup' - system of several balances in order to measure forces. Both our wind tunnels were closed circuit wind tunnels. The Force setup could not be safely used in a $Re > 80000$ because it started to flap with a significant amplitude, resulting not only in measurement errors but also overall construction tension. So, in order not to harm the setup, the experiments are performed with the $Re = 80000$. Also, every experimental run was performed by step changing in the AoA and keeping one angle for at least 50 measurement iterations in order to get rid of undesirable inertia effects.

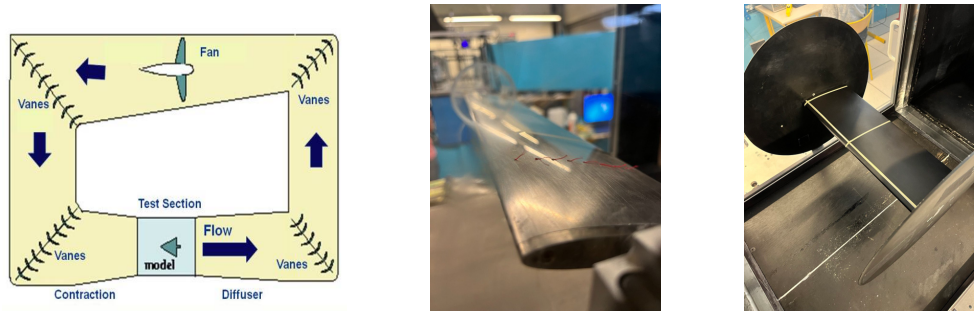

(a) Wind tunnel layout (b) 'Pressure setup' (c) 'Force setup'

Fig. (1) Experimental setup

B. Repeatability Verification

By restarting the wind tunnel several times and testing the C_l at the same Reynolds number at the same AoA, also measuring the C_l at different Reynolds numbers, the repeatability of the wind tunnel experiment and the error range can be verified. It can be seen that after taking into account the human error and the error of the wind tunnel itself, the measurement error of the C_l should be within 0.5 (2).

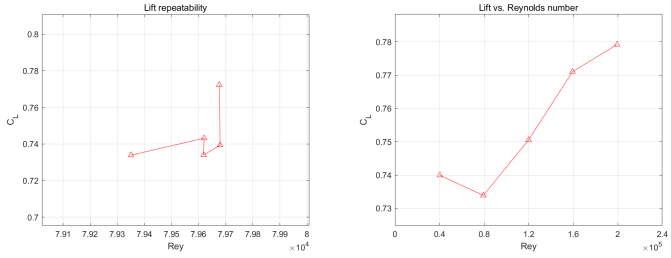

Fig. (2) Repeatability test

III. Computational Setup

All simulations are performed in the proven commercial software STAR-CCM+.

A. CFD Models

The k-omega SST model is one of the more advanced RANS models available today. It combines the advantages of the k-omega and k-epsilon models, using different strategies in the farfield and the near-wall region, respectively, to give a better prediction for the case researched in this report. Gamma ReTheta model is a single-equation transition model that gives a prediction of the laminar to turbulent transition to some extent. Considering that the airfoil will be mostly in laminar flow at 80,000 Reynolds number and the flow will undergo a laminar-to-turbulent transition, these two models are used for the simulation of the airfoil at this low Reynolds number condition.

B. Mesh Convergence Study

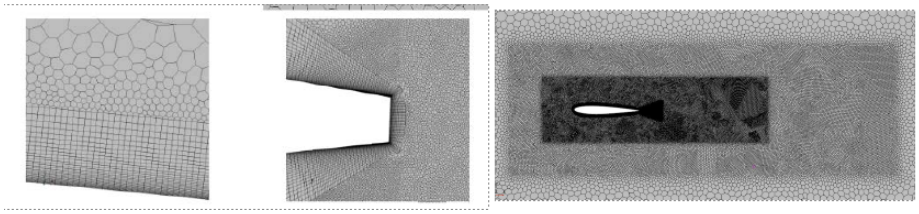

Fig. (3) Mesh Setup

Mesh-independence verification is performed for the clean configuration. The computational domain is set to 10c upstream and 20c downstream, as shown in Fig. 3. The Reynolds number is set to 80000, the same as the experiment. The prismatic layer mesh was used near the wall and the mesh refinement around the airfoil was performed. The number of cells 1e4, 2e4, 8e4, 8e4, 1.8e5, 3.3e5 were tested using the steady k-omega SST and Gamma-ReTheta model at AoA = 2°, respectively. At all these setup, wall y+ is proved to be smaller than 1. Considering the balance between computational cost and accuracy, the mesh number of 1.8e5 was selected for subsequent calculations (4).

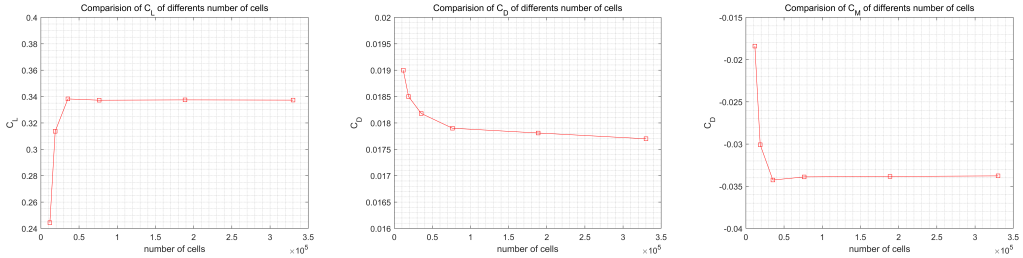

Fig. (4) Mesh Convergence Study

C. Time Convergence Study

The selected mesh is then tested with different time steps. Only the variation of the drag coefficient with time step is investigated due to its slowest convergence speed. The results show that a time step of 1e-4s is sufficient to obtain a good prediction of the force coefficient (5).

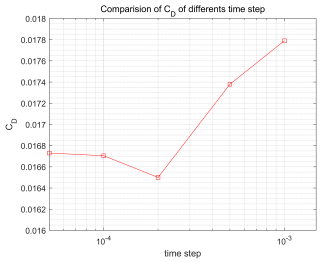

Fig. (5) Time Convergence Study

IV. Results and Discussion

A. Clean NACA-0012 Airfoil

1. Experiment

In the case of clean airfoil we had 2 test rigs - Pressure and Force. We conducted experimental work on both rigs by varying the angles of attack and the noting their subsequent variations of various aerodynamic coefficients such as C_d, C_l, C_p and C_f. The plots of those variations gave us a good understanding of the stall, drag, pressure and force characteristics of the NACA0012 airfoil and act as a baseline of comparison for the other flow control techniques and their effects on the airfoil by comparing their trends to the base.

2. CFD

On the basis of the mesh convergence study, the NACA0012 airfoil geometry was meshed (See Fig.3). Also, the y^+ wall distance is maintained less than 1 throughout the airfoil. 2D simulations were performed both with Steady and Unsteady solvers with angle of attack being varied from 0° to 15° AoA, although the computation ceases to converge after 12° AoA as the separation becomes too large.

3. Analysis

From Figure 1 it is evidently clear there is no inherent difference between the CFD Steady and Unsteady results as they seem to overlap each other, so henceforth for the NACA0012 Steady computation has been used. Another interesting phenomenon to note here is the higher lift that the CFD computation produces in comparison to the Experimental one but it also stalls earlier, and in terms of drag CFD has lower drag as expected given the previous result and Experimental of course has higher. This could be explained by either us having not the best mesh and it being too refined or CFD being a 2D computation and our experiment being a 3D one hence some addition drag as is the case.

From figure 6 C_p variations in both CFD and Experimental follow the same trend, and the seperation bubble is clearly visible moving from the trailing edge to the leading edge - growing, plateauing and seperating. Similarly for C_f seperation bubble is visible and follows the same trend. The stall/separation can be clearly seen in the CFD Figure 7, the difference between AoA 10° and 11° where according to Figure 1 the stall takes place.

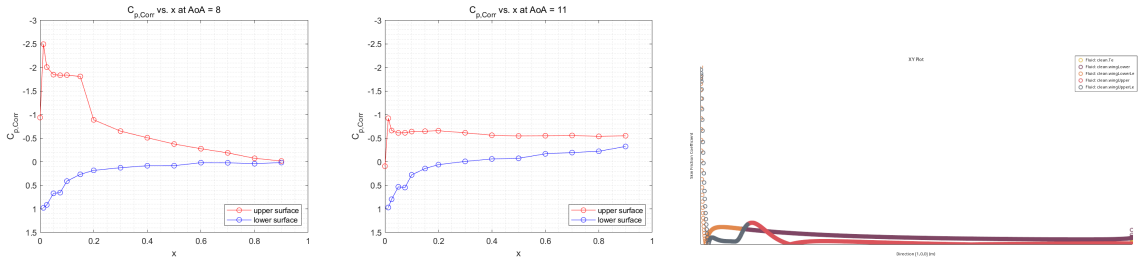

(a) C_p at 8°AoA (b) C_p at 11°AoA (c) C_f at 10°AoA

Fig. (6) C_p and C_f variations

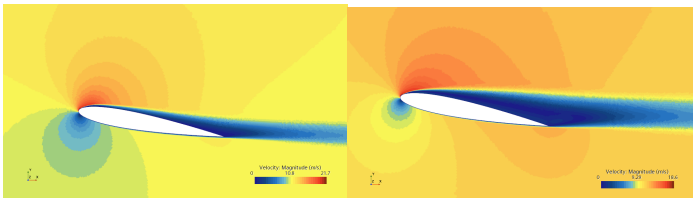

(a) Aoa = 10° (b) Aoa = 11°

Fig. (7) CFD Separation visible after 10° AoA

B. Boundary Layer Tape

1. Experiment

Two boundary layer tapes of both 0.4mm thick and 3mm wide are taped at 5% and 10% of chord respectively in an attempt to trigger the transition. The boundary layer thickness is estimated to be 0.46 mm at 5% chord length by using the empirical equation for the laminar boundary layer. Therefore the boundary layer tape has a theoretical chance of giving enough disturbance to trigger a transition. The install position of the two tapes, one in front and one behind, is also designed to give sufficient assurance of triggering a transition.

2. CFD

A geometry containing the boundary layer tape was built, rather than a clean one with simply a turbulence suppression, in the hope of studying in more detail how the boundary layer tape acts on the flow. A series of 2D simulations were performed with basically the previously tested mesh strategy. Near the boundary layer tape, the local mesh is encrypted to compensate for possible inaccuracies caused by the coarse mesh due to the degradation of the prismatic layer mesh.

3. Analysis

The results showed that the airfoil with boundary layer tape did not have better aerodynamic performance than the clean airfoil in fig.8. The results of the CFD simulations also did not match the experimental results, but instead showed similar deviations from the previous CFD results for the clean airfoil.

Taking AoA = 2° as an example, further observation of the flow field reveals the generation of a laminar separation bubble. This indicates that the flow does not go through a transition immediately after passing by the tape as expected, but continues to maintain laminar until near the trailing edge. Inspection of the pressure coefficient distribution and friction coefficient distribution

(**??**) at this AoA shows that the airflow passing by the tape does not change significantly compared to the clean configuration.

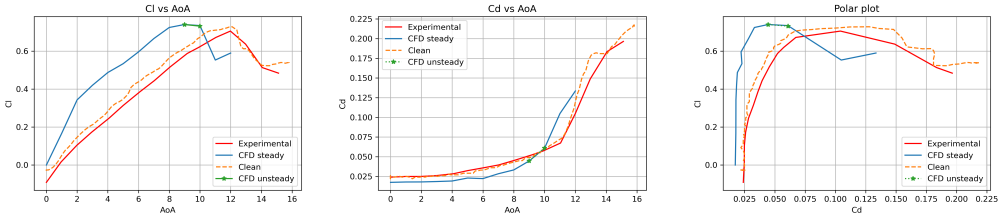

(a) Lift coefficient (b) Drag coefficient (c) Lift drag polar

Fig. (8) Results of the boundary layer tape

Taking AoA = 2° as an example, further observation of the flow field reveals the generation of a laminar separation bubble. This indicates that the flow does not go through a transition immediately after passing by the tape as expected, but continues to maintain laminar until near the trailing edge. Inspection of the pressure coefficient distribution and friction coefficient distribution (9(a)(b)) at this AoA shows that the airflow passing by the tape does not change significantly compared to the clean configuration.

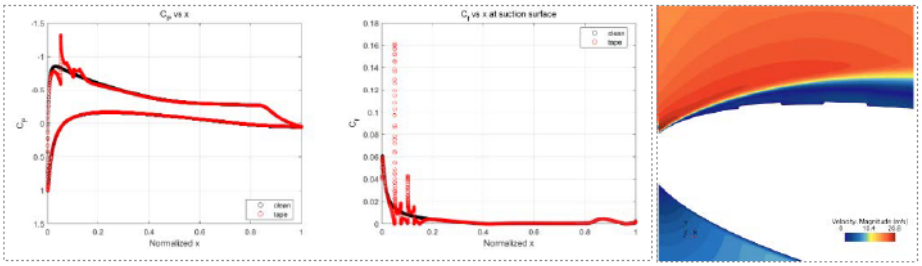

Fig. (9) (a) Cp Plot, (b) Cf plot, (c) Flow near the tape at Aoa-10

Inspection of the flow near the tape (9(c)) reveals that there is no visible disturbance at low AoA, and at high AoA the airflow passes directly over the tape from a distance. Although RANS is not able to give a correct prediction about the transition caused by small geometrical changes, the combination of experiments and simulations shows that the tape does not successfully trigger the turn. For such a low Reynolds number, the boundary layer tapes tested are still too thin to trigger the transition.

C. Cylindrical tube

1. Experimental study

A cylindrical tube of 3mm, which is thicker than the boundary layer tape, is used to force trip the boundary layer at 5% of chord (See Fig.10) because the previous attempts were unsuccessful. The tube is firmly positioned with tape both chord and span wise to make sure it won't lift off the airfoil surface and act as a slat. As the experiments are done on two different models, the tube diameter is normalised with chord to understand in future the effect of thickness of tube.(d/c is 0.03 for pressure rig model and CFD, 0.025 for force rig model.)

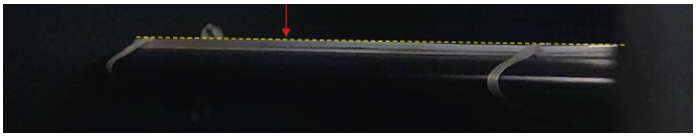

Fig. (10) Experimental model showing tube on airfoil

Through experiments, variations of C_p along the chord for a AoA range 0° to 15° (stall) is obtained. The data shows a flat C_p graph on suction surface downstream of chord with little variations at the leading edge, upstream where the tube is placed. (See fig.11) This could either suggests the flow is laminar or there is a huge separation downstream of chord.

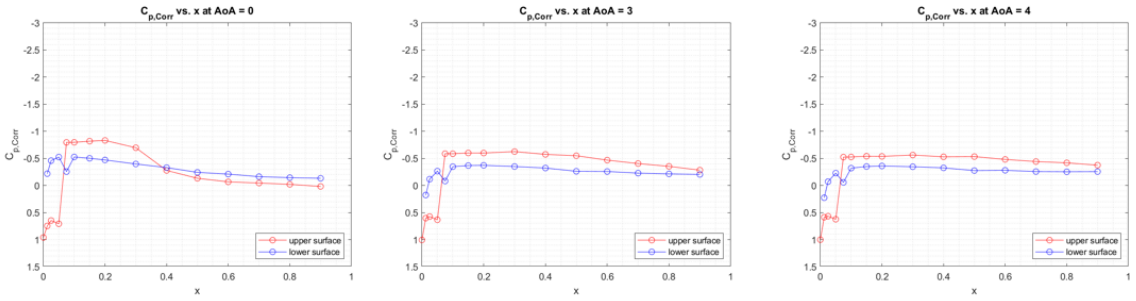

Fig. (11) Variation of C_p

The C_p variations are integrated to compute the C_L and the the same experiment is performed with the force-rig setup to obtain the C_L. A similar trend was observed from the data. A small rise, then a drop which suggests stall, but there is raise in C_L as AoA increases (See fig.12). This phenomenon of increase in C_L is hypothesised as pure force acting on the model and not an aerodynamic lift.

2. Comparison of Experiment and CFD results

To test the hypothesis flow visualization is necessary, so a numerical study of the model is performed. The numerical model used is a steady, implicit, second-order K-omega SST. Though the study is in transitional Reynolds's number range, a turbulent RANS model is used instead of transition model because we predicted forced huge separation because of cylindrical tube, from the experimental data. The C_L from the numerical study predicted the same trend of rise, drop and rise as in experiments (See fig.12).

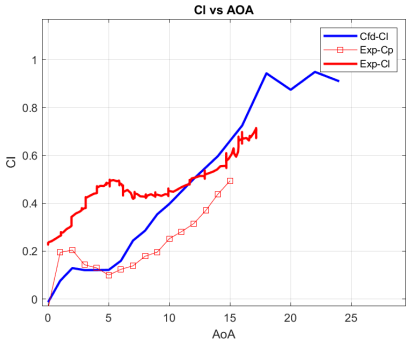

Fig. (12) Comparison of variation of C_L vs AoA

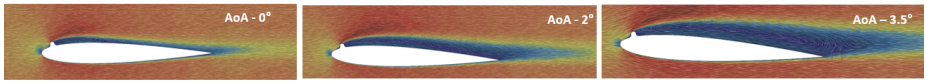

Fig. (13) Instants of Velocity contours

At AoA range of 6°-18° a huge separation and transition from study to unsteady vortex is observed Though the numerical study is a steady case and the qualitative analysis on wake cannot be trusted, it is good enough for flow visualization. But still the AoA range attributes to the rise in C_L graph though there is huge separation which could only be the case in which the additional lift that is observed is not aerodynamic lift but just a force action on the airfoil. This means once the airfoil is stalled (initial drop in C_L), as AoA increases it do not act as airfoil instead act as a flat plate creating a higher instability which can not be controlled.

D. Gurney flap

Gurney flap is a small vertical tab that is installed to the TE pressure side. The Gurney flaps of numerous different geometries are being used to achieve optimum performance under diverse design environments. These geometries differ in accordance to the installing angle, position and their shapes but the main idea of this flow control method is to sufficiently increase the lift of an airfoil by modifying the Kutta condition.

1. Experiment

Going to the experimental part, we used a 3D-printing in order to manufacture this device. Figure 14 represents the *GF* 3D model that was used in our experimental setup. The height of this flap was 2% of the chord, i.e. 2.4 mm. However, we couldn't install only a small flap because it would not be fixed properly on a *TE*, so we decided to make a little step for which this device would be taped to the airfoil.

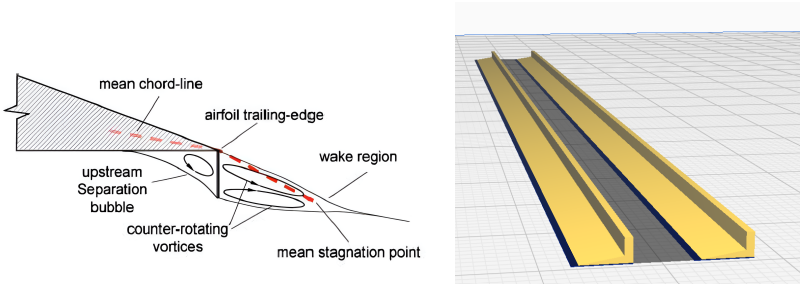

(a) Flow scheme around Gurney flap (b) Printing model

Fig. (14) Schematics of Gurney flap

2. CFD

2D CFD simulations were performed with the mesher setup that was described earlier. The wall y^+ value with this setting is below 1 for the vast majority of the airfoil. The steady solver was used because of the absence of unsteady phenomena, imposed by the *GF* and the total number of 11 simulations for the AoA=(0°,10°)

3. Analysis

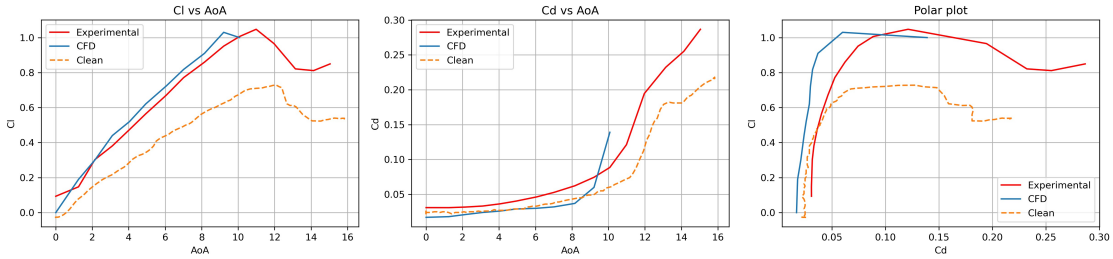

Fig. (15) Gurney flap's graphs

From the plots above it is apparently that the Cl has a noticeable rise for the case of the airfoil with GF. Nevertheless there is also increase of Cd that was imposed by the GF presence. It is also noteworthy to mention that our CFD simulations have a really good matching with the experimental results, thus we could rely on its results.

E. Serrations

A passive flow control method entitled as leading-edge serrations is inspired by the morphology of humpback whales that have large, rounded protuberances or tubercles located on the leading edge. This bio-inspired technique has been investigated for different purposes experimentally or numerically. For example, Wang and Zhuang [3] designed a modified wind turbine blades with sinusoidal wave serrations employed on the leading edge to control the boundary layer separation. The goal of this flow control method it to improve the post-stall characteristics of an airfoil by energizing the flow at the LE, thus creating 2 counter-rotating vertices on the wing's suctions side.

1. Experiment

For the experimental setup a serrations attachment to the wing was printed. From [3] we can obtain that the best flow performance can be found in the case with the serration wave amplitude of $h = 0.025c$ and wave length $\lambda = 0.33c$. During the experimental run we noticed a significant improvements in the wing's behavior after AoA of 10°, where clean wing started to flap with a big amplitude (probably due to oscillating lift, caused by the Leading Edge Vortex development), wing with serration remained totally stable even at $AoA = 20°$.

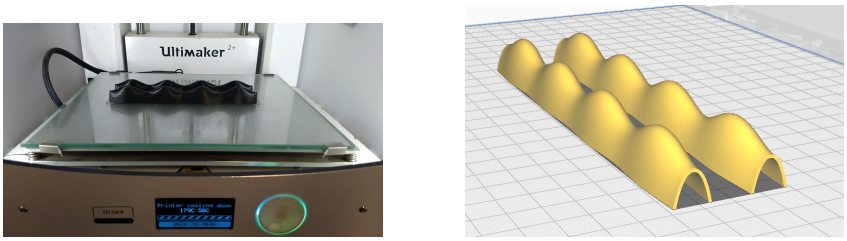

(a) Printed serrations (b) Ready-to-print model

Fig. (16) Serrations

2. CFD

Because of the fact that Serrations impose pure 3D effects that are also time-dependent [4], we had to perform 3D unsteady simulations with mesh settings and time-step described earlier and the simulation time of 0.2 seconds. However, 3D unsteady computations are very time- and power-consuming (each simulation had been running for 1.5 days on Rainman) we decided to perform only 5 simulations for AoA=(9°,13°). All the values for the upcoming plots were the mean values after the transition end at approximately 0.1 second.

3. Analysis

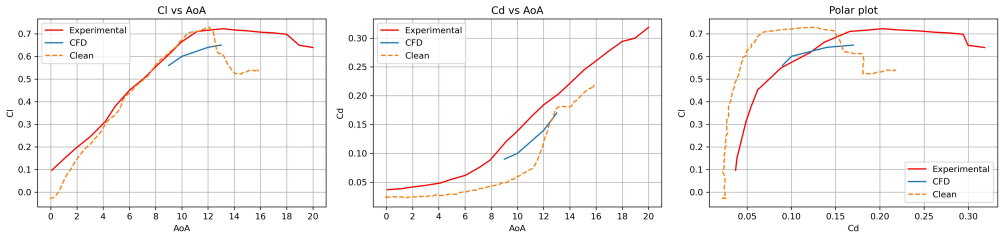

Fig. (17) Plots to Serrations

From the Fig.17 one can clearly notice that indeed, while barely changing the Cl, and increasing the Cd for the pre-stall conditions, Serrations have a huge advantage for the AoA after 12°. We could also notice that our simulation results also have a good correspondence between experimental ones. From the flow visualization on LE Serrations, from the results presented in Fig. 18 we could find that indeed, 2 counter-rotating vortexes appear just after the leading edge that delayed the the flow separation.

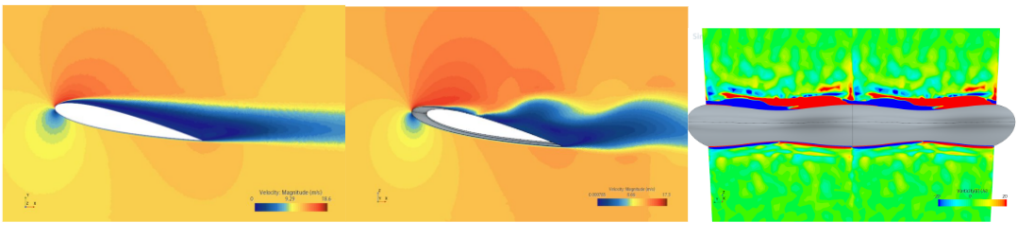

(a) Clean NACA at AoA=11° (b) Serrations peak plane at AoA=11° (c) Streamwice vorticity

Fig. (18) Scalar fields for Serrations

F. Vortex Generator

1. Experiment

The geometry of the vortex generator is made by the same 3D printing method described previously. The geometrical details are shown in Fig.19. Its height is 3mm and it is taped at 10% of the chord length from the leading edge.

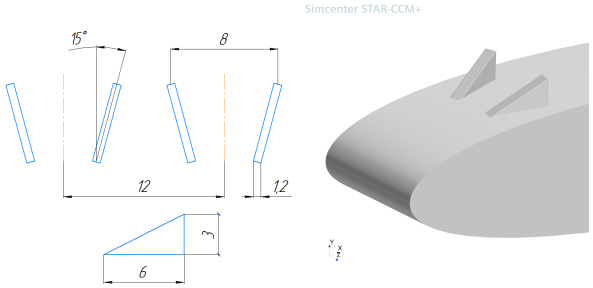

Fig. (19) Geometrical set up

2. CFD

Only one unit of vortex generators is modeled for the simulations because these vortex generators are periodically affixed to the wing. Periodic boundary conditions are used in the simulations to save computational cost. The previously tested 2D mesh setup is not strictly used, while the number of cells is appropriately reduced to 3.3 million to fit our computational resources. The mesh is shown as Fig.20.

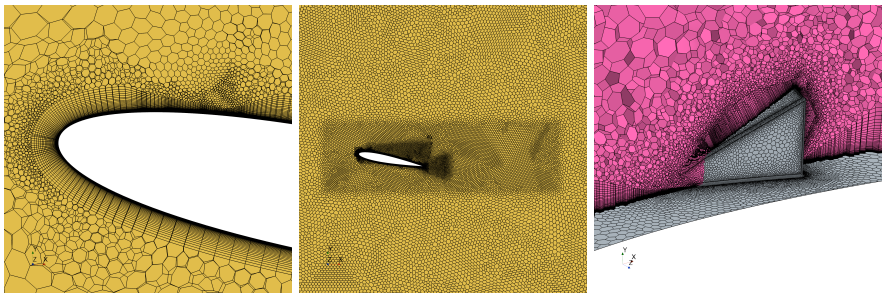

Fig. (20) Mesh set up

3. Analysis

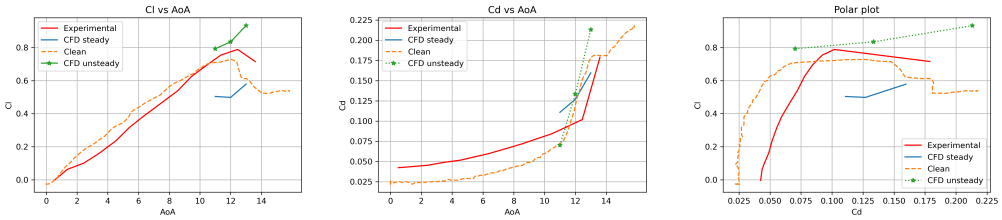

(a) Lift coefficient (b) Drag coefficient (c) Lift drag polar

Fig. (21) Results of the vortex generator

As shown in Fig. 22, the vortex generator causes a very large AoA range of C_l reduction, with only a small $C_{l,max}$ boost at the stall phase. For the C_d, there is an overall increase with the installation of the vortex generator. Observing the streamlines at AoA = 11° under the steady simulation, the airflow passes directly over the vortex generator from a distance, making the vortex generator completely covered by the massive separation flow area. Further observation of the transient streamlines and stream-wise vortex distribution under the unsteady simulation shows that the vortex generator does have a certain perturbation effect on the flow, causing the energized flow

to hit the suction surface behind the generator, resulting in a low-pressure area and increasing the lift. This also explains the great difference in the prediction of lift coefficients between steady and unsteady simulations.

As a result, the vortex generator was oversized, which caused a dramatic increase in drag and did not stimulate turbulence of the right intensity. The installation position is also further back, making it more difficult to maintain control of the airflow at high AoA conditions.

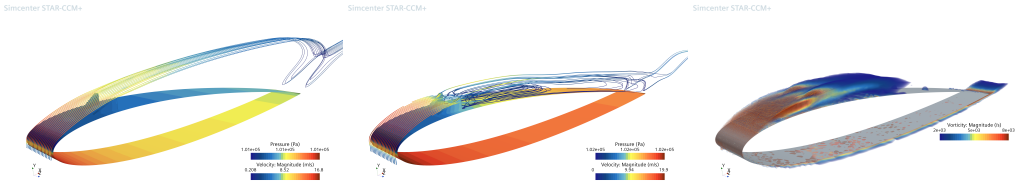

(a) Steady streamlines (b) Transient streamlines (c) Transient vorticity

Fig. (22) Flow of the vortex generator at AoA = 11°

V. Conclusion

A variety of flow control methods are verified both experimentally and by CFD. After analyzing the presented and more unpresented experimental data, among all gurney flap effectively increases the lift by modifying the Kutta conditions at the trailing edge. Serrations effectively enhance the kinetic energy of the airflow by creating vortices at the leading edge using the span-wise pressure difference, allowing the airflow to remain attached at high AoA and improving the post-stall performance. The boundary layer tape tested, however, is too thin to trigger a turbulent transition, and thus no aerodynamic performance improvement was gained. The diameter of the cylinder is too large, resulting in uncontrollable massive separation. The tested vortex generators are too large and disturb the flow field severely, greatly increasing the drag but only gaining a small improvement in $C_{l,max}$. Its installation location may not be close enough to the LE to be useful at large AoA.

To summarize, there are two main ideas behind these approaches. The first is to add kinetic energy to the airflow, either by triggering the transition early or by creating vortices to delay separation, delay stall, and improve high AoA performance. Another is to improve the Kutta conditions at the trailing edge to increase the lift.

References

[1] Mustafa Serdar Genç, Kemal Koca, Hacımurat Demir and Halil Hakan Açıke, 'Traditional and New Types of Passive Flow Control Techniques to Pave the Way for High Maneuverability and Low Structural Weight for UAVs and MAVs.'

[2] Zhu B, Huang Y, Zhang Y, 'Energy harvesting properties of a flapping wing with an adaptive Gurney flap.' Energy. 2018;152:119-128

[3] Wang Z, Zhuang M. 'Leading-edge serrations for performance improvement on a vertical-axis wind turbine at low tip-speed-ratios.' Applied Energy. 2017;208:1184-1197

[4] Zhaoyu Wei,T. H. New, 'An experimental study on flow separation control of hydrofoils with leading-edge tubercles at low Reynolds number', August 2015,Ocean Engineering; 108:336-349